Scientific Report 2007

Institute for Energy Research-
Safety Research and Reactor Technology (IEF-6)

Safety Research for Nuclear Waste Disposal

Contents:

Modeling of a prompt gamma neutron activation system for non-destructive determination of toxic elements in radioactive waste packages

J. Kettler, Y. Bai, E. Mauerhofer, R. Nabbi, R. Odoj

Institute of Energy Research (IEF-6), Forschungszentrum Jülich GmbH
Corresponding author : e.mauerhofer@fz-juelich.de

Abstract

For the determination of toxic metals in radioactive waste drums, a non-destructive analytical technique based on Prompt-Gamma-Neutron-Activation-Analysis (PGNAA) is in development at the Institute of Energy Research (IEF-6,Safety Research and Reactor Technology). A simulation study of a PGNAA system with a 14 MeV neutron generator was carried out using the MCNP-5 Monte-Carlo-Code to investigate the correlation between the gamma emission rate of certain elements and the hydrogen concentration in a large concrete sample. The limits of detection of some toxic elements were calculated for a 50 L drum filled with dry concrete. Furthermore the experimental hall with the PGNAA system and the surrounding labs were modelled in detail to calculate the neutron and photon dose rates at various locations of interest with the MCNP dose function and data from ICRP 60.

Introduction

Low and intermediate radioactive waste (LILW) may contain toxic substances like heavy metals. The final storage of LILW containing such toxic components must comply with the regulations defined by the German authority and their properties need to be taken into account for a safe disposal. Thus the amount and type of chemically toxic elements in radioactive waste must be determined. The limiting values set by the Federal Office of Radiation Protection (BfS) [1] for the final disposal in the mine Konrad are shown for some toxic metals in Table 1.

Tab. 1. Limiting quantity of some toxic metals for the final storage in disposal Konrad.

Element	***Disposal [kg]***	***200 L Drum [g]***	***50 L Drum [g]****
B	844000	557,1	139,3
Ti	18400000	12145,2	2036,3
Zn	539000	355,8	88,95
As	337	0,22	0,055
Cd	182000	120,8	30,2
Hg	43,7	0,02	0,005
Pb	33400000	22046	5511,6
Th	11600	7,7	1,91
U	23500	15,5	3,88

*For comparison with the detection limit calculated in this work

For the determination purpose a non-destructive method based on Prompt-Gamma-Neutron-Activation-Analysis (PGNAA) is in development at the Institute of Energy Research of Research Centre Jülich (FZJ). The PGNAA is an analytical technique which is based on the gamma spectrometric detection of prompt gamma radiation emitted simultaneously due to the neutron capture (Figure 1). In comparison to conventional Neutron Activation Analysis (NAA) no knowledge of the half-life of the radionuclide is necessary that allows the identification and characterization of any element in the sample. Furthermore the sample will not be destroyed, the neutron irradiation will not change the elemental composition and no sample preparation for an investigation is required [2].

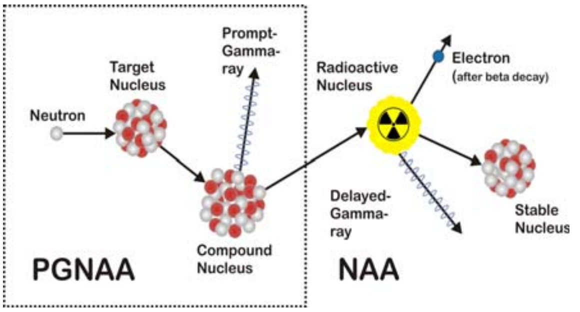

Fig. 1: The reaction scheme shows the different between PGNAA and NAA. The time between neutron capture and emission of the prompt gamma ray ranges from 10^{-12} to 10^{-16}s.

The neutron self-attenuation and the gamma-ray self-attenuation result in a non-linear problem, which may be solved by the Fix-Point Iteration method [3] in order to determine the elemental composition of the waste drum. This method is based on an iterative comparison between measured and MCNP (Monte-Carlo-Code) [4] calculated count rates of gamma rays of interest detected in the prompt gamma spectrum assuming a homogeneous density distribution.

Objectives

MCNP-simulations were carried out to study the variation of gamma emission rate of some selected elements by varying the hydrogen content in a reference concrete sample. The limit of detection for the elements given in Table 1 in a drum homogeneously filled with dry concrete were determined. Furthermore for the aim of radiation protection the MCNP model was used to determine the dose rate around the PGNAA device.

Experimental

The PGNAA drum assay system consists of a graphite interrogation chamber, a deuterium-tritium (D-T) accelerator neutron source (14 MeV neutrons, 10^8 n/s strength) [5] for irradiation of the waste drum and a high-purity Germanium detector (100% rel. efficiency) for the measurement of prompt gamma radiation (Figure 2). The wall of the graphite chamber is about 50 cm thick, which is used as a shield to protect the environment of the experiment against neutrons as well as a reflector. In order to reduce fast neutron damage, the detector is arranged perpendicularly to the neutron generator and is shielded with LiF resp. Li_2CO_3. The PGNAA drum assay system is set up in a 12 m x 4.8 m experimental hall with 85 cm thick baryta concrete walls.

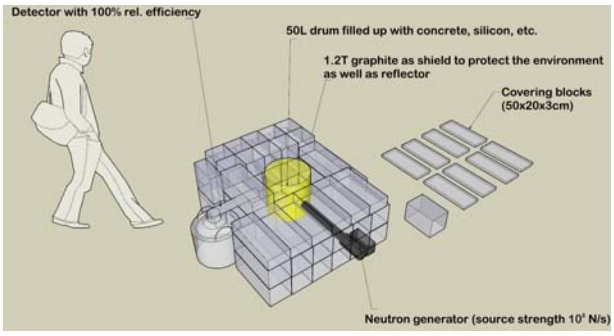

Fig. 2: 3D-Modell of the PGNAA drum system.

Computational method

In order to optimize the geometry of the PGNAA system the prompt gamma spectrum and the neutron flux at the detector surface were first investigated for different detector/ neutron source configurations and a large concrete sample (115 kg) using MCNP-5. For neutron and photon transport calculations the standard libraries ENDF/B-VII and JEFF 3.1 were used. In the MCNP input-file a disc geometry was assumed for the neutron source emitting 10^8 n/s in 4π sr. The detector crystal is described by a 8 cm x 8 cm cylinder cell containing natural germanium. The track lengths of gamma rays are simulated like in a real HPGe-detector using the so called “pulse height tally”. For the detector simulation the neutron and radiation data library JEFF-3.1 was employed. The sample is a 15 mm thick steel drum, homogenous filled with dry concrete with the following concentration: H(0.5558 wt%), O (49.8076 wt%), K (1.9239 wt%), Al (4.5746 wt%), Si (31.5092 wt%), S (0.1283 wt%), Ca (8.2941 wt%), Fe (0.2147 wt%), Na (1.7101 wt%) and Mg (0.2565 wt%). The mass of the sample is 115 kg. In order to simulate samples with higher H-content, the fraction of oxygen was continuously replaced by hydrogen. For the dose rate calculations the experimental hall with the surrounding labs was modelled in detail. The simulations were performed using the MCNP dose function as well as data from ICRP 60. In every simulation run 10^9 particle histories were calculated resulting in high statistical precision in term of relative error and variance of variance (vov), which remained within the accuracy intervals (1 σ value of 0.2 %). The MCNP simulated prompt gamma spectrum of the large dry concrete sample is shown in figure 3.

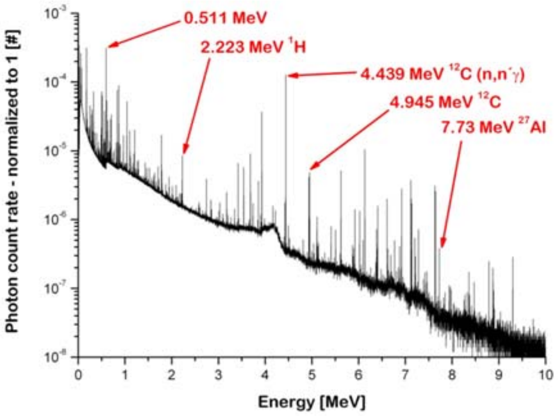

Fig.3 : MCNP simulated prompt gamma spectrum of the dry concrete sample (115 kg).

Results

The dependence of the gamma emission rate for Al (7.725 MeV), Si (4.935 MeV) and H (2.223 MeV) with the H-concentration of the concrete sample is shown in Figure 4.

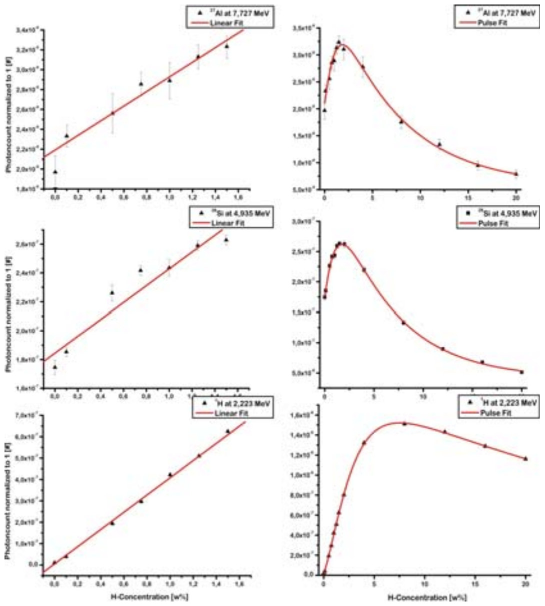

Fig. 4: Gamma count rates of aluminium, silicon, and hydrogen as a function of the H-concentration in the concrete sample.

Accordingly the count rate increases linearly for a H concentration lower than 1.6 wt%. A further increase of the H-concentration in the sample leads to an exponential decrease of the gamma activity of aluminium and silicon due to the thermal neutron capture by hydrogen. This finding is in agreement with the result of reference [6]. In the case of hydrogen the gamma yield decreases linearly due to of the increase of hydrogen concentration. The dependence of the gamma emission rate of C (4.945 MeV) in the graphite chamber with the H-concentration of the sample is shown in Figure 5.

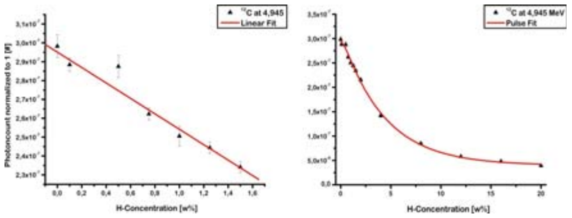

Fig. 5: Gamma count rate of carbon in the graphite chamber as a function of the H-concentration in the concrete sample.

We observed that the gamma count rate of C decreases for an increasing H-concentration as a result of the moderation of the fast neutrons in the sample. Consequently the signals of C and H are appropriate for monitoring the mean thermal flux in the sample. Knowledge on the moderation properties are essential for the estimation of the thermal neutron flux in the sample. The neutron thermalization as well as the neutron absorption influence the neutron activation of the sample and may reduce the gamma ray emission affecting so the detection limit of the system

The detection limit m_{Limit} of the PGNAA system for a dry concrete sample (50 L) was calculated as follows [7]:

$$m_{Limit} = \frac{M}{a \cdot N_{av}} \cdot \frac{3.92 \cdot \sqrt{2 \cdot N_U / t} + 0.5 \cdot 3.92^2 / t}{\sigma_{th} \cdot \Phi_{th} \cdot I_\gamma \cdot \varepsilon_\gamma} .$$

M is the molar mass, a the abundance, N_{av} the Avogadro number, N_{U} is the underground count rate, t the measurement time, σ_{th} is the thermal neutron cross section, I_γ the intensity of the gamma line and ε_γ is the photo-peak efficiency for the dry concrete sample. Calculations with MCNP show that the mean thermal neutron flux inside the 50 L concrete drum is approximately ϕ_{th} = 32000 n/s/cm^2. The limits of detection calculated for the elements given in Table 1 and for a irradiation/ counting time of 900 s are presented in Table 2.

The limit of detection for the elements investigated in this study are lower than the limiting values set by BfS except for thorium, uranium, arsenic and mercury. For comparison, the limits of detection of ^{232}Th and ^{238}U obtained by the gamma scanning of a 200 L drum filled with concrete and a counting time of 1 hour are 10 g and 50 g respectively. In the case of arsenic and mercury, the limiting quantities set by the BfS for the total waste volume to be disposed in Konrad are very low (337 kg for As and 43.7 kg for Hg).

Neutron and photon dose rates were calculated for radiation protection purposes at various locations around the experimental hall for two configurations of the PGNAA device (Figure 6). The results shown in table 3 demonstrate that the photon dose rates are negligible in comparison to the contribution of neutrons. The neutron dose rates depend on the alignment of the PGNAA device i.e. on the orientation of the neutron generator. For the existing configuration the calculated dose rates remain below 2,3 µSv/h, that is prescribed by Federal Office for Radiation Protection (BfS) as a limit for a radiation exposed working person.

Tab. 2. Detection limits for the elements of Table 1, calculated with relation (1) for a 50 L drum filled with dry concrete.

Isotope	***M [g/mol]***	***a [%]***	***σ_{th} [b]***	***E□ □□[eV]***	***I□ [%]***	***N_U [s^{-1}]***	***□□$\tilde{x}i$□ (abs)***	***m_{Limit} [g]***
^{10}B	10,81	19,9	3837	0,478	93,3	3,9	16,9	0,0002
^{48}Ti	47,87	73,7	5,81	6,76	48,8	0,02	19,4	0,019
^{64}Zn	65,39	48,6	0,76	7,86	13,1	0,006	16,4	0,85
^{75}As	74,92	100	4,5	6,81	12,4	0,02	19,4	12,45
^{113}Cd	112,90	12,2	20600	0,558	73,9	2,3	17,3	0,053
^{199}Hg	198,97	16,9	2150	0,367	91,3	4,4	16,4	0,75
^{207}Pb	206,98	22,1	0,712	7,37	78,8	0,006	17,8	111,20
^{232}Th	232,04	100	7,37	0,969	1,8	0,9	21,2	791,51
^{238}U	238,06	99,3	2,68	4,06	5,5	0,13	26,6	237,69

Tab. 3 Neutron and photon dose rates at different places of interest (see Fig. 5.)

Place of interest	***Neutron dose rate [µSv/h]***		***Photon dose rate [fSv/h]***	
	orient. 1	orient. 2	orient. 1	orient. 2
Outside of the sliding gate – 1	0.0346	0.3113	0.00045	0.00148
Way of walking outside of the hall – 2	0.0179	0.0083	0.00019	0.00012
Adjoining laboratory – 3	0.0050	0.0153	0.00021	0.00039
Lead window to look inside the hall – 4	0.0236	0.0104	0.00022	0.00011

Conclusions

For the certain elements selected in this work for coupled neutron and gamma transport analysis a linear correlation between the gamma emission rate and a hydrogen concentration in the sample was determined for the concentration range of 0 – 1.6 wt%. This reflects an increase of the thermal neutron flux in the sample. For higher concentrations the gamma count rate decrease exponentially due to the increasing neutron capture of hydrogen i.e. a decrease of the thermal neutron flux. Limits of detection of some toxic elements obtained for 50 L filled with dry concrete were compared with the limiting quantity set by the BfS for the final disposal of radioactive waste in Konrad. Dose rate calculations with MCNP-5 using the activation and gamma data library ENDF/B-VII and JEFF 3.1 show that the radiation exposure at various locations outside the experimental hall are lower than the limits prescribed by the Federal Office for Radiation Protection (BfS) for radiation exposed person.

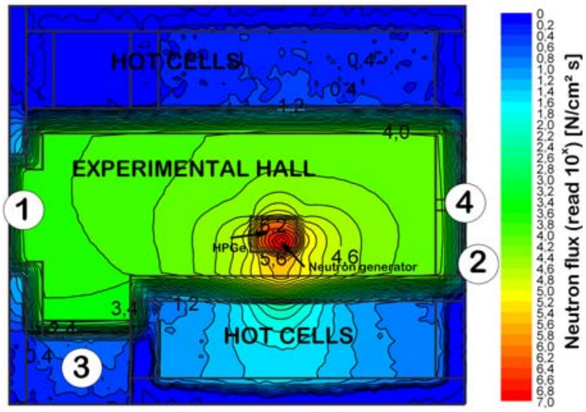

Fig. 6: Total neutron flux (0 - 14 MeV) contour plot for the PGNAA device (orientation 1) in the experimental hall. The scale values are the exponents of the neutron flux (7 reads as 107). The location of the dose rate calculations are given by the number in the circles (see Tab. 1). In orientation 2 the PGNAA model of the measurement setup was 90° rotated in clockwise direction relative to orientation 1.

Outlook

The PGNAA measurements of 20 L and 50 L reference drums homogeneously filled with concrete and known amount of heavy metals (Pb, Cd, Hg) will be perform in order to validate our MCNP-code. The effect of an inhomogeneous density distribution of the waste matrix on the gamma count rate will be study by MCNP. Furthermore, a parameterization of the thermal neutron flux for various waste compositions will be carry out using MCNP.

References

[1] Bundesamt für Strahlenschutz: Planfeststellungsbeschluss für die Errichtung und den Betrieb des Bergwerkes Konrad in Salzgitter. 2002.

[2] Molnár, Gábor L.: Handbook of Prompt Gamma Activation Analysis. Budapest: 1. Aufl. Kluwer Academic Publishers, 2004. - 1-4020-1304-3

[3] Holloway, J.P. ; Akkurt, H.: The fixed point formulation for large sample PGNAA—Part 1: theory. In: Nuclear Instruments and Methods in Physics Research A 522 (2004) S. 13

[4] X-5 Monte Carlo Team: MCNP - A General Monte Carlo N-Particle Transport Code, Version 5. Los Alamos National Laboratory: 2003.

[5] EADS-SODERN: Neutron Generator GENIE 16 GT.

[6] Oliveira, C. ; Salgado, J. ; Carvalho, F. G.: Optimation of PGNAA instrument design for cement raw materials using the MCNP code. In: Journal of radioanalytical and nuclear chemistry 216 (1997) Nr. 2, S. 191-198

[8] Arbeitskreis SIGMA: Nachweisgrenze und Erkennungsgrenze bei Kernstrahlungsmessungen; Zählende hochauflösende gammaspektrometrische Messungen ohne Berücksichtigung des Probenbehandlungseinflusses. 1993.

Radionuclide retardation by Mg-Al-Cl-layered double hydroxide, identified as crystalline phase component of the corrosion products of research reactor fuel elements

H. Curtius, B. Hansen, G. Kaiser, Z. Paparigas

Institute for Energy Research (IEF-6), Forschungszentrum Jülich GmbH
Corresponding author : h.curtius@fz-juelich.de

Abstract

At the Institute for Energy Research (IEF-6,Safety Research and Reactor Technology) the behavior of non-irradiated and irradiated UAl_x-Al and U_3Si_2-Al dispersed fuel elements in repository relevant aquatic phases is under investigation. As repository relevant aquatic phases a salt brine ($MgCl_2$-rich brine 2 solution), granite water (Äspö-type) and clay pore water (Mont-Terri-type) are used. Both non-irradiated fuel types corroded completely in these aquatic phases within one year. Identical investigations performed with irradiated fuel elements show the same corrosion behavior in salt brine. The investigations in granite and clay pore water are still in progress. Due to the corrosion radionuclides are mobilized first and then immobilized by the formed corrosion products (secondary phases). In order to understand the radionuclide retardation processes (sorption and incorporation) the identification of the phase components is a requirement. Up to now a lesucite and a Mg-Al-Cl-layered double hydroxide (LDH) were identified as crystalline phase components. It was possible to fix di- and trivalent element-species by incorporation irreversible in the lattice structure of the Mg-Al-Cl-LDH. Sorption investigations with the Mg-Al-Cl-LDH and with a Mg-Al-Eu-Cl-LDH were performed with different repository relevant radionuclides in salt brine and in clay pore water. In future work all crystalline phase components need to be identified and their ability to retard radionuclides will be investigated.

Introduction

In deep geological formations a safe disposal of highly radioactive waste can be achieved. The concept includes a multi barrier system which shall isolate and immobilize the radioactive waste additionally.

Irradiated research reactor fuel elements are classified as highly radioactive waste. Here the fuel containment and the fuel itself are regarded as technical barriers while the closure material of the gallery represents the geotechnical barrier. The area including these two barriers of a final repository is described as near field. The host rock and overlaying rock represent the geochemical barriers and are described as far field of a final disposal.

At present three research reactors, the FRM-II-reactor (München), the FRG-I-reactor (Geesthacht) and the BER-II-reactor (Berlin) with a thermal output higher than 5 MW are in operation in Germany. In these reactors dispersed U_3Si_2-Al-fuel is used. In general, three possible back-end options for irradiated research reactor fuel elements exist in Germany [1]: first, irradiated research reactor fuel elements of USA origin can be sent back when these fuels were taken out of the reactor not later than May 2006. This affects basically the dispersed metallic UAl_x-Al-fuel, which was used in the FRJ-II-reactor (Jülich) till May 2006. Secondly, reprocessing in Great Britain or France is possible and it will performed with respect to economical reasons. Thirdly, dry interim storage and later on, direct disposal in deep geological formations has been taken into account too. As deep geological formations salt, granite and clay are considered. In granite and clay formations pore water is always present whereas in a salt repository a water ingress and subsequent formation of salt brines is considered as accident scenario.

At the Institute of Energy Research (Safety Research and Reactor Technology, IEF-6) investigations to the behavior of research reactor fuel elements in these repository relevant aquatic phases are performed. The work is focused on the near field phenomena [2].

Objectives

The retardation of mobilized radionuclides by the secondary phases is of main interest, because these phases represent the first barrier in view of further radionuclide mobilization in the near field. It is essential to identify and qualify each phase component and consequently to gain informations of the radionuclide retardation processes at a molecular level.

Retardation processes can be described by sorption and incorporation mechanism. Investigations with the identified crystalline phase component, a Mg-Al-Cl-LDH were started. The ability of this compound to incorporate and sorb radionuclide species in repository-relevant aquatic phases is under investigation and first results are presented in this paper.

Experimental

The experimental set-up for the syntheses of the Mg-Al-Cl-hydrotalcite is described in [3]. Incorporation experiments were performed with di- and trivalent element species. As trivalent element species europium and samarium and as divalent element species cadmium were chosen. The used amounts of Eu and Sm were fixed to 10 % of the molar amounts of Al, while the used amount of Cd was fixed to 3.33% of the molar amount of Mg.

Sorption experiments were performed according to the batch-technique. All samples were stored in glass tubes with occasional shaking under argon-atmosphere for two days. Then all samples were filtered (450 nm) and the pH was measured. Aliquots of the solutions were analyzed radiometrically. The solids were washed, dried and analyzed by XRD and FT-IR. Blank experiments were performed too, indicating that the sorption on the glass walls was negligible.

Results

In order to obtain informations about the radionuclide retardation processes, secondary phases obtained after total corrosion of non-irradiated UAl_x-Al- and U_3Si_2-Al-fuel element samples in salt brine were analyzed. A Mg-Al-layered double hydroxide (LDH) with chloride as interlayer anion was identified as a crystalline phase-component [2]. In Figure 1 the crystal structure of a Mg-Al-Cl-LDH is shown.

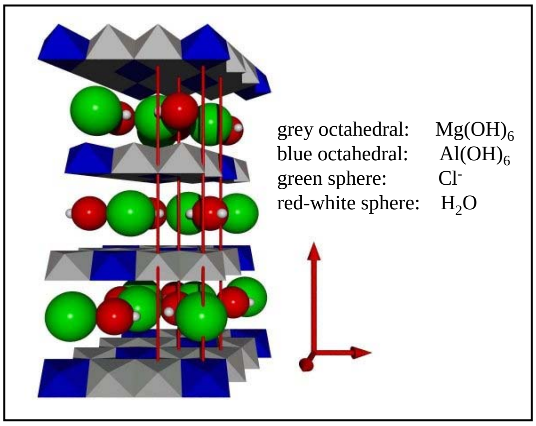

Fig. 1 Crystal structure of a Mg-Al-Cl-LDH

One possibility to retard element species irreversible is to **incorporate** these species in the lattice structure. With regard to the lattice structure of the LDH it should be possible to incorporate di- and trivalent element species through substitution reactions with the divalent Mg or the trivalent Al.

According to the co precipitation method incorporation investigations were performed. First, trivalent element species were chosen for substitution of the trivalent Al. The obtained solids were analyzed and for Eu-III the formula can be derived as:

$[Mg_3Al_{0.94}Eu_{0.099}(OH)_8]\,Cl_{0.98}\,(CO_3^{2-})_{0.02}\ 5.79\ H_2O$

Details are given in [4]

For Sm the formula can be derived as:

$[Mg_3Al_{0.91}Sm_{0.092}(OH)_8]\,Cl_{0.93}\,(CO_3^{2-})_{0.037}\ 1.93\ H_2O$

and details are given in [5]

First results using Cr and Ce as trivalent element species show that a substitution of Al is possible too.

In conclusion it is possible to exchange the trivalent Al by other different trivalent element species. It should be pointed out that the ionic radii of Al is 0.51 Angström and the range of ionic radii of the used elements was in the range of 0.61 to 1.034. Hence it is possible to bring element species in the lattice structure of the Mg-Al-Cl-LDH within this range.

In a next step a partial exchange of the divalent Mg was aspired. As element species cadmium was chosen. The ionic radii of Mg is 0.65 while the ionic radii of Cd is0.97 Angström. The obtained solid was analyzed and the formula can be given as:

$[Mg_{2,62}Al_1Cd_{0,08}(OH_8)]\,Cl_{0,76}\,(CO_3)_{0,12}\ 4,28\ H_2O$

Further investigations with divalent iron are in progress.

Another possibility to retard element species is given by **sorption**. Due to the structure of this Mg-Al-Cl-hydrotalcite (Fig.1) an anion exchange in the interlayer should be possible. We performed sorption experiments according to the batch technique and as repository relevant element species, iodine, pertechnetate and selenite [6] were chosen. It was aspired to determine the sorption capacities on a Mg-Al-Cl-LDH and on a Mg-Al-Eu-Cl-LDH in water, in the repository relevant $MgCl_2$-rich brine solution and in clay pore water. Especially the influence of the larger europium-III ion, which represents in the Mg-Al-Eu-Cl-LDH about 10% of the molar aluminium amount, was of interest. A similar sorption behaviour on both LDHs was observed for iodine and pertechnetate in water. The retardation processes were identified as ion exchange mechanism. In clay pore water and in $MgCl_2$-rich brine iodine and pertechnetate were not retarded.

Fig. 2 shows the temporal dependence of selenite sorption with an initial concentration of 4.28 10^{-13} mole/L in water on the Mg-Al-Cl-LDH.

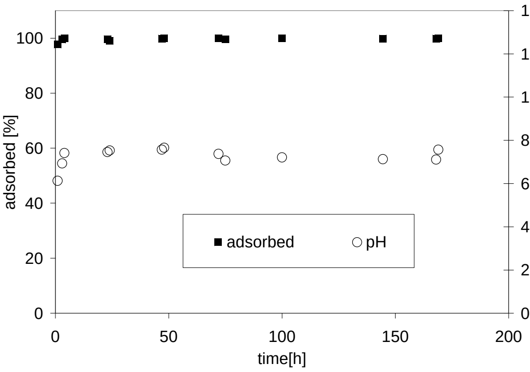

Fig. 2 Time dependent sorption of selenite on Mg-Al-Cl-LDH in water

Equilibrium was reached within a couple of hours. Selenite adsorbed quantitatively, corresponding to an anion exchange capacity of 2.14 10^{-14} mole/g. The equilibrium pH was about 7.5. The same results were obtained with the Mg-Al-Eu-LDH. Then, identical investigations were performed in clay pore water and in $MgCl_2$-rich brine. In clay pore water selenite sorbed similar on both LDHs and sorption values of 60 % were reached corresponding to an anion exchange capacity of 1.28 10^{-14} mole/g. In $MgCl_2$-rich brine selenium sorbed only up to 20 % corresponding to an anion exchange capacity of 0.43$10^{-14}$ mole/g. The same tendencies were found for the sorption on the Mg-Al-LDH. The equilibrium pH values in $MgCl_2$-rich brine were 4.5. It should be mentioned that the pH-values in $MgCl_2$-rich brine were not corrected. For a correction Grambow et al. showed that a factor of about 1.89 must be added to the measured values. This would mean that in $MgCl_2$-rich brine the pH-values are about 6.5. For the decrease of the selenite exchange capacities in the sequence salt brine, clay pore water and pure water two possible explanations can be given. **First** the influence of pH. Time dependence sorption investigations with selenite were performed on both LDHs in water and in clay pore water while the initial pH-values were adjusted between pH 4 and pH 8. In $MgCl_2$-rich brine the initial pH-values were adjusted between pH 4 and pH 6. In water and in clay pore water the equilibrium pH-values of about 8 were determined while the pH-values for the $MgCl_2$-rich brine were about 5 (corrected pH-value is 6.89) (Fig. 3).

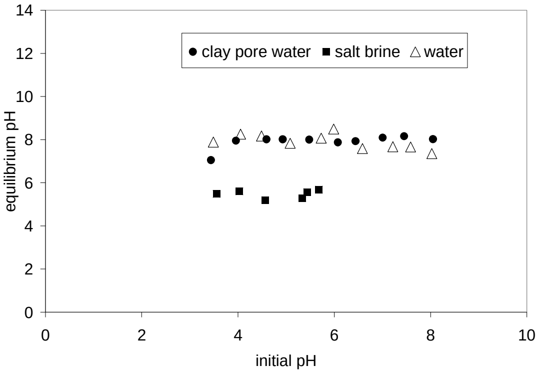

Fig. 3 Initial and equilibrium pH-values for the sorption of selenite in water, clay pore water and salt brine on the Mg-Al-Eu-Cl-LDH

Same results were obtained for the Mg-Al-Cl-LDH. Comparing these initial and equilibrium pH-values, we suppose that the LDHs must have high pH buffering capacities and that there is no difference between both LDH types. Nevertheless these results indicate clearly that in the investigated initial pH-ranges the sorption does not depend on pH.

Secondly the observed decrease in sorption with increase in ionic strength of the used aquatic phases can be explained by the high amounts of chloride present. In water where no competition anion is present, the used molar amounts of selenite were exchanged quantitatively. The clay pore water contains 0.29 mole of chloride anions. In comparison to the used molar amounts of selenite, the chloride anions represent a molar excess of about $1.5 \cdot 10^{+12}$. This effect is more drastic for the $MgCl_2$-rich brine, which contains about 9.75 mole of chloride anions, representing a molar excess of about $1.5 \cdot 10^{+13}$. Investigations performed by J. Das showed that 30% of phosphate (trivalent anion) was removed while working with a chloride solution, which contained only an equivalent molar concentration of chloride with respect to phosphate. Our results agree with these observations and it is obviously that high amounts of chloride as competition anions reduce the ion exchange capacities of the LDHs. Nevertheless, our results obtained for the sorption of selenite in $MgCl_2$-rich brine showed although, that even under the conditions of final disposal in a salt dome, when the presence of a $MgCl_2$-rich brine is predicted, selenite will be retarded by both LDHs.

Time dependence sorption investigations with selenite were performed with LDH concentrations of 0.1g/L instead of 10g/L too, but no sorption of selenite was observed.

XRD analysis of the solids, carried out to ensure that no structural changes of the LDHs occur especially in consequence of pH treatments, showed the typical 003, 006, 009 and 110 reflexes. The lattice parameters, in particular the basal parameter c, had not changed. A possible explanation for the invariant c parameter is that the exchange reaction between chloride as interlayer anion and selenite takes place only at the edges of the interlayers. For LDHs, possible adsorption sites are located within the interlayer and onto external surfaces. Quantitative information on which sites are occupied can be obtained from the adsorption isotherms, linear adsorption isotherm indicating an ion-exchange mechanism. If the isotherm is no longer linear and reaches a plateau, then this part can be assigned to the adsorption on external sites.

In the present work, the adsorption isotherms were obtained by plotting the amount of selenite sorbed on LDHs, Cads, against the selenite concentration in solution at equilibrium, Ce.

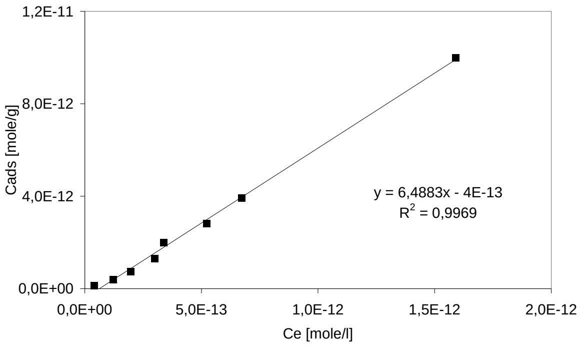

Fig. 4 Adsorption isotherm of selenite in salt brine on Mg-Al-Eu-Cl-LDH

Fig. 4 shows the adsorption isotherm for selenite adsorbed at pH 4.5 (pH value not corrected) on the Mg-Al-Eu-Cl-LDH at 25°C. The obtained isotherm was linear and the same results were obtained for the isotherm with the Mg-Al-Cl-LDH. We therefore assume that the favoured reactions in our system are ion-exchange processes. The sorption data for selenite in the concentration range used were analysed in terms of the Freundlich equation. Freundlich isotherms often describe sorption of trace amounts of sorbing species satisfactorily. The Freundlich equations give satisfactory fits to the experimental results (R^2 = 0.9909 for the Mg-Al-Eu-Cl-LDH and 0.9977 for Mg-Al-Cl-LDH). The linear regressions of the plots give slopes of about 1, indicating that a concentration independent, i.e., a linear adsorption of selenite on both LDHs exists in the concentration range used. The results of the Freundlich equations for the sorption of selenite in clay pore water are similar. Then all data of the isotherms were fitted to the Dubinin-Radushkevich (D-R) equation and the mean energies of sorption were calculated. The mean energy of sorption is the free energy change when one mole of ion is transferred to the surface of the solid from infinity in the solution. The values of the mean energies of the sorption in $MgCl_2$-rich brine for both LDHs were found to be 12.9 kJ/mole, which is in the range for ion exchange reactions (8-16 kJ/mole) [7].

In clay pore the calculated values of the mean energies are identical to be 12,9 kJ/mole water and the DR-plot for the sorption of selenite on Mg-Al-Eu-Cl-LDH is represented in Fig. 5.

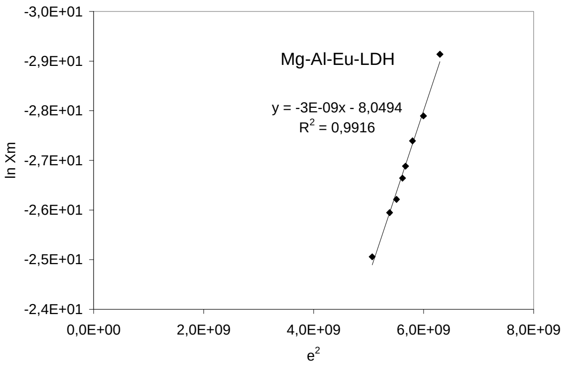

Fig. 5 DR plots of selenite sorption on Mg-Al-Eu-Cl-LDH in clay pore water

The maximum sorption capacities were then calculated by the intercept point of the functions with the ordinate. The sorption capacities in clay pore water are $4{,}53\cdot10^{-5}$ mole/g for Mg-Al-Cl-LDH and $3.19\cdot10^{-4}$ mole/g for Mg-Al-Eu-Cl-LDH. For the Mg-Al-Eu-Cl-LDH the maximum sorption capacity in $MgCl_2$-rich brine was found to be $4.54\ 10^{-5}$ mole/g, and for the Mg-Al-Cl-LDH a value of $3.28\ 10^{-5}$ mole/g was obtained. These values are very similar but do not reach the calculated maximum anion exchange capacities for divalent anions ($1.4\cdot10^{-3}$ mole/g for Mg-Al-Cl-LDH and $0.9\cdot10^{-3}$ mole/g for Mg-Al-Eu-Cl-LDH). A possible explanation is that the ion exchange processes only take place at the edges of the interlayer mainly due to the high amounts of chloride anions present.

Conclusions

In order to gain informations about the retardation processes of the radionuclides with the formed secondary phases, investigations in salt brine, clay pore water and in water were performed. Retardation by **sorption** was investigated

with the identified crystalline phase component, a Mg-Al-Cl-LDH and with a Mg-Al-Eu-Cl-LDH.
Iodine, pertechnetat and selenite were chosen as repository relevant radionuclide. The results could be summarized as follow:

- only in water iodine and pertechnetat were retarded similar by boths LDHs via an ion exchange mechanism
- selenite was retarded by both LDHs in water, in clay pore water and in salt brine
- equilibrium was reached within 5 hours
- sorption was uneffected by pH (range 3-8)
- chloride influence the sorption of selenite
- retardation can be described by ionic exchange mechanism
- sorption is not influenced by the amount of europium present in the Mg-Al-Eu-Cl-LDH

Retardation of radionuclides by **incorporation** was investigated too. It was possible to substitute the divalent Mg and the trivalent Al by different di- and trivalent element species.
In conclusion the Mg-Al-Cl-LDH and the Mg-Al-Eu-Cl-LDH can retard mobile radionuclide species via sorption and incorporation mechanism even in repository relevant aquatic phases.

Outlook

Our work is focussed on the near field phenomena of final disposed research reactor fuel elements. After corrosion of the fuel the mayor point of interest is to describe the radionuclide interactions with the secondary phases because these secondary phases represent the first barrier in view of radionuclide mobilisation. In future work we aspire to

- identify all secondary phase components
- describe their thermodynamic properties
- describe their interactions with radionuclide species at a molecular level

References

[1] G. Thamm: Disposal of Irradiated Fuel Elements from German Research Reactors – Status and Outlook- in Trans. Int. Conf. Research Reactor Fuel Management (RRFM 1999), Belgium, 159 (1999)

[2] H. Curtius, et al., Untersuchungen zum Verhalten von Forschungsreaktor-Brennelementen in den Wirtsgesteinsformationswässern möglicher Endläger, Jül-4237, Jülich, ISSN 0944-2952 (2006)

[3] H. Curtius and Z. Kattilparampil, Sorption of iodine on Mg-Al-double layered hydroxide, Clay Minerals, **40**, 455 (2005)

[4] T. Stumpf , H. Curtius , C .Walther , K. Dardenne , K. Ufer , T. Fanghänel, Incorporation of Eu(III) into hydrotalcite: a TRLFS and EXAFS study, Environ Sci Technol.;**41 (9)**, 3186-91, 2007
and
Hilde Curtius ; Kristian Ufer, Eu incorporation behavior of a Mg-Al-Cl layered double hydroxide, Clays and Clay Minerals, **55** (4), 354 - 360 , 2007

[5] K. Ufer, R. Kleeberg, J. Bergmann, H. Curtius, R. Dohrmann, "Refining realstructure parameters of disordered layered structures within the Rietveld method", Size-Strain V, Diffraction Analysis of the Microstructure of Materials,
7 to9 October, 2007, Congress-Centre Garmisch-Partenkirchen, Germany

[6] H. Curtius, Z. Paparigas, G. Kaiser, Sorption of selenium on Mg-Al and Mg-Al-Eu layered double hydroxides, Transactions, p. 66, Migration 2007, 26 to 31 August 2007 in München, Germany

[7] Khan S.A:, Reman R-U, Khan M.A., Journal of Radioanalytical and Nuclear Chemistry, **190**, 81 (1995)

Fabrication of zirconia based ceramics by internal gelation for conversion of trivalent actinides

G. Benay, G. Modolo
Institute for Energy Research, Safety Research and Reactor Technology, Forschungszentrum Jülich GmbH
Corresponding author : g.modolo@fz-juelich.de

Fabrication of fuels or targets for transmutation of minor actinides (MA) requires a dust-free process. Such a requirement can be fulfilled by sol-gel methods, which allow the production of microsphere precursors. Internal gelation, one of these methods, was studied at IEF-6 in collaboration with the CEA Marcoule. A study of the parameters involved in internal gelation (essentially the quantity of organic additives urea and hexamethylenetetramine HMTA present in the initial solution) was performed. Afterwards, the effects of these parameters on the structural evolution of the microspheres during thermal treatment were studied. It was observed that the structure and density of the microspheres are heavily dependant of the quantity of organic precursors present in the initial solution. Urea in particular has been found to bring porosity to the material, in addition to its catalytic effect on HMTA decomposition. The elimination of these organic compounds is however a major issue which causes the formation of cracks on the microspheres if no optimization is performed.

Partitioning and Transmutation and Partitioning and Conditioning are two promising methods for management of spent nuclear fuel [1]. In both cases, a suitable material is required to contain minor actinides retrieved from partitioning. Research on such a material is mainly aimed towards Inert Matrix Mixed Oxide fuels (IMMOX), and among them is yttria-stabilized zirconia especially promising [2].

In addition to the formation of a solid solution with tetravalent actinides, interesting properties of this matrix include small neutron capture cross section, high melting point, and high radiation and chemical stability.

The sol-gel methods present a great interest in the preparation of such matrices: the wet chemistry suppresses the formation of dust and is simple enough to be remote handled. Internal gelation in particular is technically very simple, and has therefore been chosen in this study. This process produces small beads or kernels, which can be directly used as a fuel after sintering (SPHEREPAC process) [3]. It requires however optimizations to ensure good mechanical properties of the material. Moreover, the precise role of the organic precursors used (hexamethylenetetramine HMTA and urea) is not totally clear.

Gels and kernels of ceria-doped yttria-stabilized zirconia were prepared and characterized [4] with a specific focus on the role of urea and HMTA, and on the effect of thermal treatment on the material obtained. The pressing of kernels into pellets was also studied.

Zirconium oxychloride, yttrium nitrate and cerium nitrate were dissolved in deionized water at room temperature, with a total concentration of 1.6 mol/L and a composition of 76% Zr, 14% Y and 10% Ce. HMTA and urea were dissolved with different concentrations in a second solution. Equal volumes of both solutions were then mixed at 3°C to prepare a broth, the cooling step being needed to prevent premature gelation. Broths compositions are defined by the ratios R_U and R_H, corresponding to the molar ratios of urea on metal and HMTA on metal, respectively. Kernels were then prepared by dropping broths through a nozzle into silicone oil heated at 90°C. The kernels were afterwards washed and dried at room temperature overnight prior to thermal treatment (see Fig. 1). Some calcined kernels were pressed into pellets with a pressure of 900 MPa prior to sintering at 1600°C.

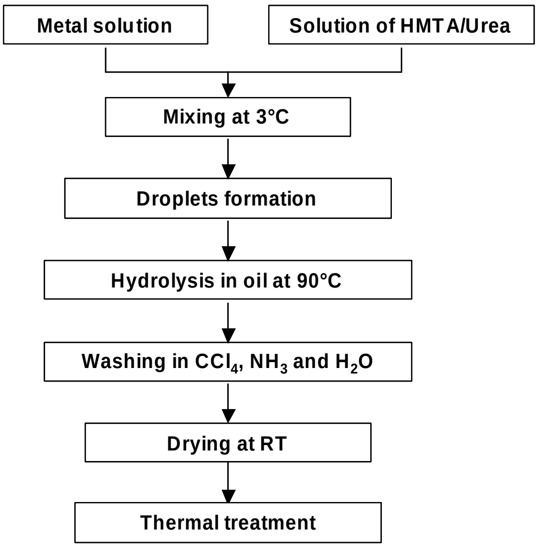

Fig. 1: Flowsheet of kernels preparation

To determine the gel properties, the viscosity of broths was measured continuously during their heating to 90°C. The results of these studies for different quantities of urea and HMTA in the broths are summarized in Figure 2. It is observed that the gelation temperature decreases when the quantity of HMTA increases, but also when the quantity of urea increases for a fixed quantity of HMTA. This indicates a catalytic effect of urea on HMTA decomposition [5]. A clear effect of urea and HMTA on gel structure is also observed. A porous structure is obtained with a high quantity of urea and a relatively low quantity of HMTA, and a dense structure otherwise. This indicates that urea is also a porosity bringer, in addition to its catalytic role.

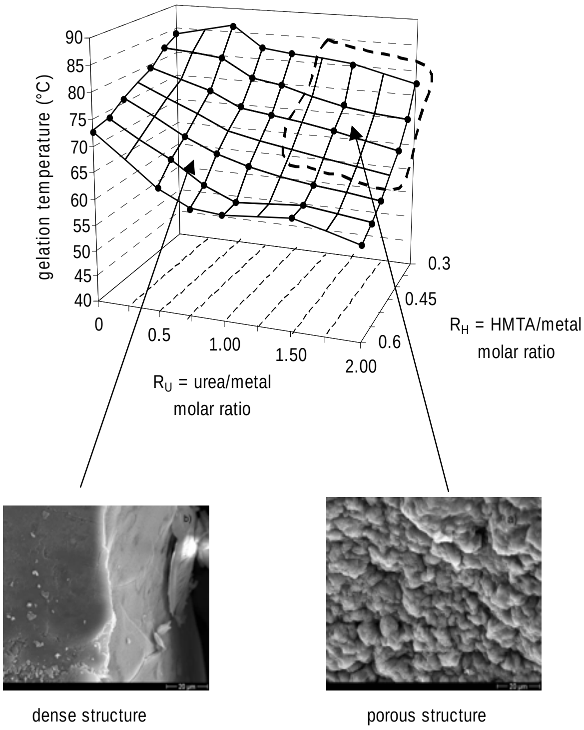

Fig. 2: Gelation temperature for different molar ratios of urea and HMTA on metal in the broth and corresponding gel structure

Kernels were prepared from broths with different concentrations of urea and HMTA. It was observed that the structure of kernels matched the structure of gels. Moreover, it was found that the quantity of urea present had an influence on the stability of the kernels during thermal treatment. They were found indeed totally broken if no urea was present in the broth, and only cracked otherwise. For kernels with a porous structure, the cracks formation only starts for temperatures higher than 110°C. Urea is therefore required to improve the mechanical properties of the kernels.

The thermal behavior of the kernels was studied by TG-DSC. Fig. 3 is typical of the curves obtained when urea is present in the broth. An endothermic mass loss is first observed from room temperature to a temperature T_1, which corresponds to the elimination of water. Afterwards, an exothermic mass loss is observed up to 400°C, with a maximum at a temperature T_2. This strong effect is associated with the decomposition of organic products issued from urea and HMTA and the probable main cause of cracks formation. Finally, a smaller exothermic effect without associated mass loss is observed at a temperature T_3.

It corresponds to a transition in the crystalline state of the material. Detailed values are available in Table I.

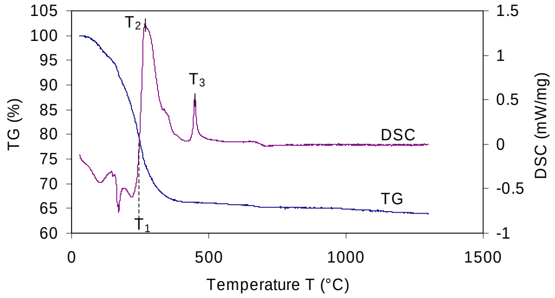

Fig. 3: Thermal analysis of kernels with urea in the broth.

Calcined kernels were pressed into pellets. A re-pressing method was used due to the observation of a berry structure on single-pressed pellets [6]. It was found that increasing the number of pressing steps increased the density of the pellet, up to 86% TD (Fig. 4). On the other hand, no clear effect of the broth composition on density was observed. An exception is the case with no urea present, with a lower density measured. This is in accordance with the improvements brought by urea on the material properties.

The structure of the pellets was studied by SEM. An important porosity was observed when no urea was present in the broth, explaining the low density measured (Fig. 5a). When urea was present in the broth, a berry structure appeared after single pressing, along with a high density inside the kernels traces (Fig. 5b). Repressing the pellet allowed to break this berry structure, but hard agglomerates remained, limiting the densification (Fig. 5c). If a broth composition corresponding to a porous gel structure was used, further pressings allowed to break these agglomerates, and also increasing the porosity. A homogeneous structure was thus observed (Fig. 5d).

TABLE I: Results of thermal analysis for the different kernels studied
a: specific heat of the first exothermic effect;
b: specific heat of the second exothermic effect

	R_H	T_1 (°C)	T_2 (°C)	T_3 (°C)	Q_1 [a] (J/g)	Q_2 [b] (J/g)
0.5	0.6	248	276	434	346	59
0.75	0.56	251	279	453	988	33
1.0	0.56	257	311	473	1408	11
1.5	0.3	247	268	449	511	47
1.5	0.4	249	288	466	986	46
2.0	0.3	236	281	458	502	62
2.0	0.4	247	286	460	921	54

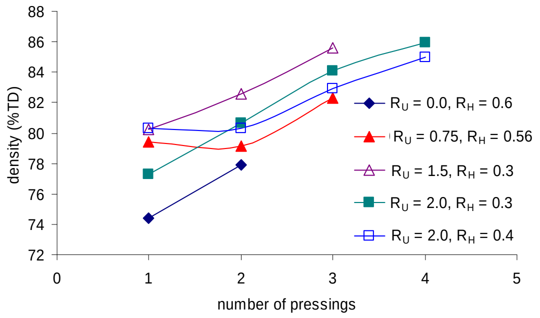

Fig. 4: Sintered densities of selected pellets with different initial compositions and numbers of pressings.

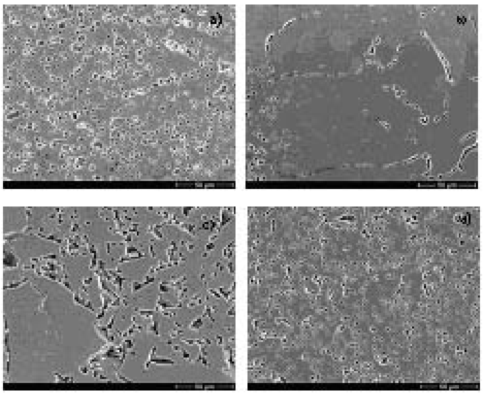

Fig. 5: Structure of pellets with different initial compositions and numbers of pressings.

Kernels of yttria-stabilized zirconia doped with ceria were prepared by internal gelation. It was found that urea had a catalytic role in HMTA decomposition, helping the gelation process, but was also able to bring porosity to the gel and improve its mechanical properties and resistance during thermal treatment. On the other hand, the mixture of urea and HMTA caused the formation of products causing a strong exothermic effect during their decomposition. This effect was responsible for crack formation. Optimizations were attempted, but could not totally solve the problem. The phenomena occurring during gelation are however now better understood.

An interesting alternative is pellet pressing. It was observed that using a repressing method was required to prevent the occurrence of a berry structure. Densities up to 86% TD were then obtained, with a homogeneous structure.

This work was supported by the European Commission (project EUROPART, contract no. F16WCT-2003-508854).

References

[1] "Actinide and fission product partitioning and transmutation – Status and assessment report," OECD-NEA 1999.

[2] A.A. Bukaemskiy, D. Barrier, G. Modolo," Physical properties of 8 mol% Ceria doped yttria stabilised zirconia powder and ceramic and their behaviour during annealing and sintering", *J. Eur. Ceram. Soc.*, **26,** 1507 (2006).

[3] Ch. Hellwig, P. Heimgartner, Y. Tomita, S. Kono, "Sphere-pac filling for irradiation tests of the FUJI project," Proceedings of the global 2003 conference, New Orleans, USA, November 16-20, pp. 1348-1353 (2003).

[4] G. Benay, F. Hubert, G. Modolo, "Preparation of yttria-stabilized zirconia-ceria kernels as fuel precursors using internal gelation", *Radiochimica Acta*, in press.

[5] J.L. Collins, M.H. Lloyd, R.L. Fellows, "The basic chemistry involved in the internal-gelation method of precipitating uranium as determined by pH measurements", *Radiochimica Acta*, **42,** 121 (1987).

[6] R.B. Matthews, P.E. Hart, "Nuclear fuel pellets fabricated from gel-derived microspheres", *J. Nucl. Mater.*, **92**, 207 (1980).

The crystallization of 8YSZ-CeO_2 powders

A.A. Bukaemskiy, G. Modolo
Institute for Energy Research, Safety Research and Reactor Technology,
Forschungszentrum Jülich GmbH, D-52425 Jülich, Germany

*Corresponding author: g.modolo@fz-juelich.de

The effect of the addition of ceria (0 – 100 %) on the thermal behaviour and crystallization of yttria cubic stabilised zirconia powders prepared by a "soft" co-precipitation method was investigated in detail using TG-DSC and XRD. It was shown that the synthesized powders after drying constitute a mixture of pure ceria and (ZrYCe)Ox solid solution with a reduced ceria content. The synthesized powders after drying with ceria contents up to 20 mol.% are amorphous. Their crystallization in the temperature range of 350 to 600 °C is accompanied by two exothermal effects, which can be explained by the crystallization of (ZrYCe)Ox solid solution with a reduced ceria content and the incorporation of ceria into this matrix respectively. The powders with a ceria content above 20 mol.% are already crystallized after drying, and a solid solution with equilibrium composition of (ZrYCe)Ox is formed during heating to 600 °C. At temperatures above 600 °C, all investigated powders form homogeneous (ZrYCe)Ox solid solutions with face-centred cubic, fluorite type structure, without any apparent segregation of ceria. The (ZrYCe)Ox lattice parameter was found to be a function of ceria content according to Vegard's law.

In recent years, yttria cubic stabilized zirconia (YSZ) has been considered as an inert matrix for burning excess plutonium from spent fuels in light water reactors [1, 2, 3] and as one of the most promising matrix for the immobilisation of actinides [4, 5, 6]. According to [7], yttria stabilized zirconia (YSZ) is the most appropriate material in comparison with the other possible alternatives, since it satisfies the criteria for inert matrix, such as phase stability over large temperature range and under severe irradiation dose; inertness with regard to transmutation products, cladding, and reactor water; small thermal neutron adsorption cross section, high leaching resistance, high radiation stability and a small neutron capture cross-section [6, 8, 9]. Moreover, YSZ has the ability to form solid solutions over a wide range of solubility with compounds such as UO_2, ThO_2, and PuO_2 and with rare-earth trivalent oxides [10].

In the experimental investigations, cerium is traditionally used as a simulant of tetravalent actinides. Cerium and plutonium have nearly identical ionic radii [11], the lattice parameters for PuO_2 (0.5395 nm) and for CeO_2 (0.5411 nm) are close together [12].

The co-precipitation method is sufficiently simple and dust-free technology, what determines its adaptability for nuclear applications [1]. The processes of elements co-precipitation and materials behaviour during calcination were investigated in detail for the pure zirconia [13, 14, 15], for the some compositions of the $ZrO_2 – Y_2O_3$ system [16, 17] and $ZrO_2 – CeO_2$ system [17, 18]. However, additional quantitative information on the evolution of the crystal structure of YSZ-based ceramic depending on the different parameters, such as actinide amount and annealing temperature, is required.

In the present work, the thermal and crystallization behaviour of the powders is studied in detail using thermogravimetry coupled with differential scanning calorimetry (TG-DSC) and X-ray diffraction (XRD). The formation of thermally stable oxide solid solution during calcination is also investigated for the whole range of ceria.

For all powders, the concentration of Y_2O_3 in the (ZrY)Ox system was kept constant at 8 mol.% (8YSZ), which determined the stabilisation of the material in the face-centred cubic, fluorite type structure.

The detailed analysis of the X-ray diffraction patterns of the investigated powders with the ceria concentrations between 33 and 100 % after drying crystallized directly in a face-centred cubic, fluorite type structure. Each Bragg reflection had a complex shape and could be approximated well by a sum of two Gaussian functions, as shown in Fig.

1a for the representative system 74-CeO_2-8YSZ. These two Gaussian functions differ in the intensity, the position and the value of the peak width. The width of the first Gaussian peak (fine line) is significantly smaller and its maximum is shifted towards lower angles compared to those of the second Gaussian peak (dotted line). With increasing ceria content, the intensity of the first Gaussian peak increases, while the intensity of the second Gaussian peak decreases. Moreover, the positions of the first Gaussian peaks remain practically constant, whereas the value of the shift ($\Delta 2\theta$) decreases due to the displacement of the second Gaussian towards the smaller angles.

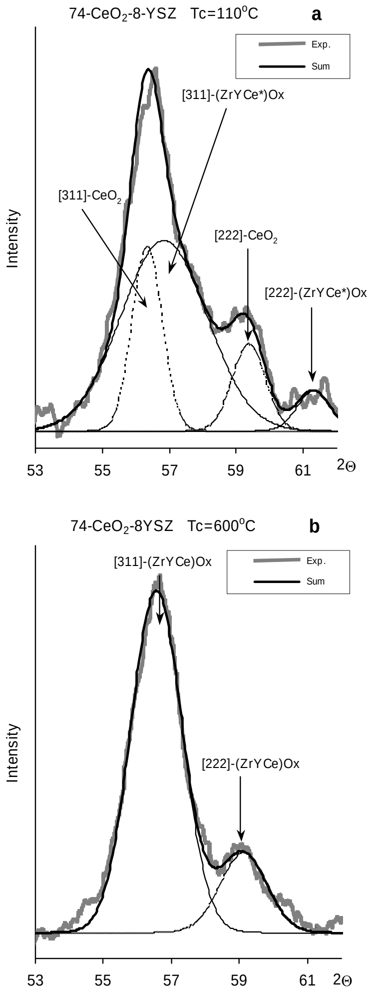

Fig. 1. Fragments of X-ray diffraction patterns of 74-CeO_2-8YSZ powder after drying (a) and after calcination at 600 °C (b).

The exact calculation of the lattice indicated that the series of the first Gaussian peaks corresponds to the pure ceria (solid triangles and horizontal dashed line in Fig. 2). In turn, the series of the second Gaussian peaks corresponds to the solid solution (ZrYCe*)Ox with the ceria content different from the initial one, shown as open triangles in Fig. 2.

For the comparison, the lattice parameter calculated from XRD patterns of the investigated powders after calcination at Tc = 600 and 1400 °C is plotted as a function of the ceria content in Fig. 2. The experimental data are well described by a linear dependence (Vegard's law) and correlate with the data for 8YSZ and pure CeO_2 from JCPDS catalogue [19, 20] and with the results presented in [21, 22, 23]:

$$a,\ \text{Å} = 2.73 \cdot 10^{-3} \cdot C_{\text{Ce}} + 5.148 \quad T_{\text{C}} = 1400\ °\text{C} \qquad (1)$$

$$a,\ \text{Å} = 2.64 \cdot 10^{-3} \cdot C_{\text{Ce}} + 5.155 \quad T_{\text{C}} = 600\ °\text{C} \qquad (2)$$

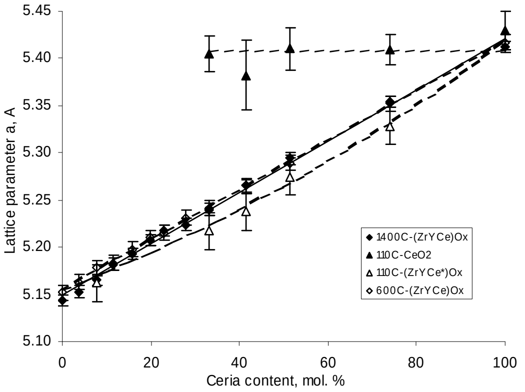

Fig. 2. Lattice parameter, *a*, for the studied powders as a function of ceria content after different calcination temperatures (Tc).

Let us assume thet the amount of the precipitated pure ceria (denoted as α in the following) is a constant fraction of the total ceria content. Considering this, the ceria content C_{Ce}* in the synthesised solid solution depends on the initial ceria content (C_{Ce}) and the amount of the precipitated pure ceria α as:

$$C_{\text{Ce}}^{*} = (C_{\text{Ce}} - \alpha\, C_{\text{Ce}})/(1 - \alpha\, C_{\text{Ce}}). \qquad (3)$$

We can therefore assume that the lattice parameter depends linearly on the ceria content in the powders after drying as well as in the powders after calcination at 1400 and 600 °C. Based on equation (2) this dependence can be written as:

$$a, \text{Å} = 2.64 \cdot 10^{-3} \cdot (C_{Ce} - \alpha C_{Ce})/(1 - \alpha C_{Ce}) + 5.155 \qquad (4)$$

Using equation (4), the parameter α was determined from the experimental data in Fig. 2, which is shown as a slanting dashed line. To calculate the parameter α, a single data point for the composition 8-CeO_2-8YSZ from the previous work [24] was taken into account in the present optimization. The optimized value of α equals 0.31. This means that 31 mol.% ceria is precipitated in the form of pure CeO_2 during co-precipitation, whereas 69 mol.% ceria is in the (ZrYCe)Ox solid solution.

The powders with a ceria content of up to 20 % are amorphous after drying as well as after calcination up to 350 °C. The Bragg reflections are sufficiently wide (B ~ 5.5 ÷ 6.5 °). The exothermic effect at the crystallisation of material is characteristic for these powders. After calcination of the powder at a temperature higher than 600 °C, the synthesized materials are solid solutions with a composition corresponding to the initial oxide contents, because their lattice parameters obey Vegard's law (Fig. 2).

The crystallization of 8-CeO_2-8YSZ and 8YSZ powders was studied in detail in the temperature range between 380 and 1600 °C. The results of the thermal analysis (TG-DSC) are shown in Fig. 3.

For the 8YSZ sample (Fig. 3a), the DSC curve presents only one exo-effect between 420 and 525 °C, which corresponds to the phase transition of the material from the amorphous to crystalline state [25, 26, 27]. For the 8-CeO_2-8YSZ sample (Fig. 3 b), the crystallisation includes two exothermic peaks. As described in Fig. 3 b, the first effect is detected between 370 °C (T_1) and 502 °C (T_3) with a maximum at 445 °C (T_2). The second effect is detected between 502 °C (T_3) and 660 °C (T_5) with a maximum at 568 °C (T_4).

According to the TG and DSC results, the 8-CeO_2-8YSZ and 8YSZ powders were calcined at 370, 450, 500, 550, 600, 800, 950, 1400 and 1600°C before XRD analysis. For powders after drying and calcination at temperatures below 370 °C (T_1), the powders are amorphous. At temperatures higher than T_1, the diffraction peak of XRD spectra reveal that the material crystallises in a face-centred cubic fluorite-type structure. For powders calcined from 450 to 950°C, diffraction lines are wider and shifted in the smaller angels region compared to those for the powders calcined at 1400 and 1600°C.

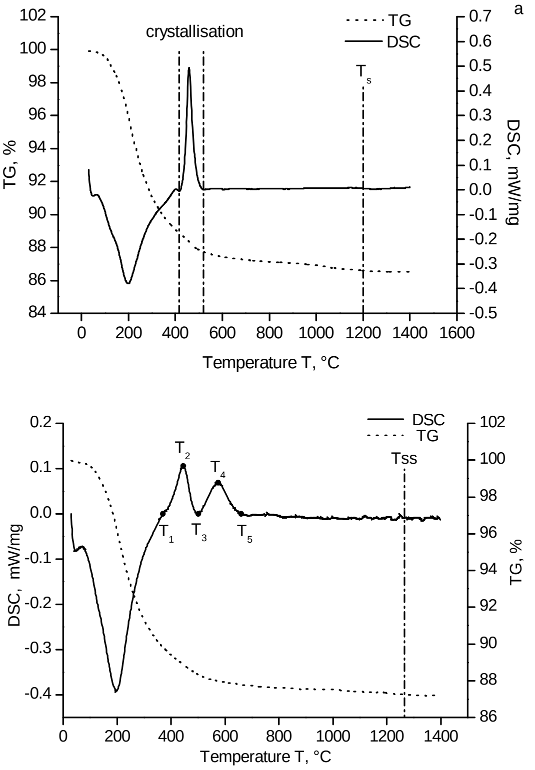

Fig. 3. TG, DSC curves of 8YSZ (a) and 8-CeO2-8YSZ (b) powders.

For the 8-CeO_2-8YSZ and 8YSZ, the dependences of the lattice parameter *a* on the calcination temperature are shown in (Fig. 4).

For the 8YSZ powder, the lattice parameter decreases with increasing calcination temperature (Fig. 4). In contrast, the 8-CeO_2-8YSZ sample calcined at the lower temperatures $T_2 = 450$ °C and $T_3 = 502$ °C do not follow the above tendencies with the calcination temperature. Their lattice parameters at these temperatures (a = 5.162 and 5.174 Å, correspondently) are significantly lower than the values at T_4. Moreover, after calcination at 450°C (T_2), the values of the lattice parameter of 8-CeO_2-8YSZ and 8YSZ are very similar and equals a = 5.162 ± 0.016 and 5.154 ± 0.009 Å, correspondently.

Hence, taking into account the TG-DSC and XRD results, the following sequence of material crystallisation can be assumed: predominant crystallisation of zirconia-yttria matrix with the ceria deficiency in the temperature range from T_1 to T_3 (first exo-effect) and incorporation of the rest of ceria in the crystal lattice in the temperature range from T_3 to T_5 (second exo-effect).

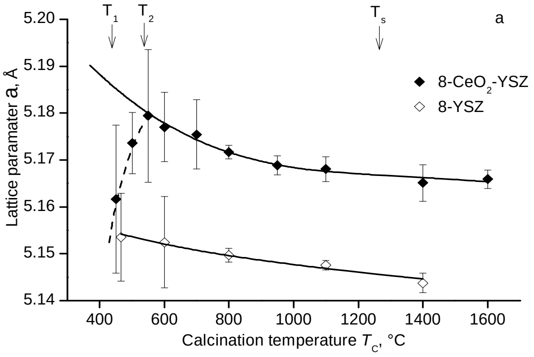

Fig. 4. Dependence of the lattice parameter with the calcination temperature of 8YSZ (a) and 8-CeO2-8YSZ powders.

As shown in Fig. 3 for the representative samples 8-CeO_2-8YSZ and 8YSZ, the significant mass loss (~ 12 %) takes place during heating from 20 to 600 °C. From 20 to 350 °C, the mass loss was accompanied by a heat consumption, which corresponds to the elimination of adsorbed gases, adsorbed and hydrated water and impurities. From 350 to 650 °C, the mass loss was accompanied by the material crystallisation from the amorphous to crystalline state. At temperatures higher than 650 °C, no thermal effects were detected. During heating from 650 to 1230 °C, the mass of the sample continued to decrease but the mass loss was negligible (smaller than 0.9 %). This can be associated with the elimination of the residual OH groups from the material [27, 24]. After annealing at temperatures higher than T_S = 1230 °C, the mass remained constant. This temperature T_S appears to be the temperature of stable solid solution formation. The precise value of T_S was determined based on the method described in [27].

The temperature of stable solid solution formation (T_S) varied with the ceria content. The temperature of stable solid solution formation (T_S) of the powders with 0 - 20 mol.% ceria is independent of the ceria concentration and equals 1230 ± 10 °C. For ceria concentrations from 20 to 28 %, T_S abruptly decreases from 1220 °C to 790 °C, correspondently. For ceria contents from 33 to 100 %, T_S remains constant and equals 775 ± 5 °C.

References

1 C. Degueldre, J.M. Paratte, J. Nucl. Mater. 274 (1999) 1-6.
2 H. Matzke, V.V. Rondinella, T. Wiss, J. Nucl. Mater. 274 (1999) 47-53.
3 C. Degueldre, J. Alloys Compd. 444-445 (2007) 36-41.
4 P.E. Raison, R.G. Haire, Prog. Nucl. Energy 38 (2001) 251-254.
5 A. Fernandez, D. Haas, R.L.M. Konings, J. Somers, J. Am. Ceram. Soc. 85 (2002) 694-696.
6 R.B. Heimann, T.T. Vandergraaf, J. Mater. Sci. Lett. 7 (1988) 583-586.
7 V.M. Oversby, C.C. McPheetes, C. Degueldre, J.M. Paratte, J. Nucl. Mater. 245 (1997) 17-26.
8 K. E. Sickafus, H. Matzke, H. Hartmann, K. Yasuda, J.A. Valdez, P. Chodak III, M. Nastasi, R.A. Verrall, J. Nucl. Mater. 274 (1999) 66-77.
9 M.A. Pouchon, M. Döbeli, C. Delgueldre, M. Burghartz, J. Nucl. Mater. 274 (1999) 61-65.
10 W.L. Gong, W. Lutze, R.C. Ewing, J. Nucl. Mater. 227 (2000) 239-249.
11 J.A. Dean, Lange's Handbook of Chemistry, 14th edition, McGraw-Hill, New-York, 1992.
12 J.G. Pepin, G.J. McMarthy, J.Am.Ceram.Soc. 64 (9) (1981) 511.
13 H.Th. Rijnten, in: Physical and chemical aspects of adsorbents and catalysts, Academic Press Inc., London, 1970.
14 R. Srinivasan, M.B. Harris, S.F. Simpson, R.J. DeAngelis, B.H. Davis, J. Mater. Res. 3 1(988) 787-797.
15 T. Sato, J. Therm. Anal. Calor. 69 (2002) 255-265.
16 O. Duran, J. Tartaj, J.F. Fernandez, M. Villegas, C. Moure, Ceram. Int. 25 (1999) 125-135.
17 A.P. Oliveira, M.L. Torem, Pow. Tech. 119 (2001) 181-193.
18 A.L. Quinelato, E. Longo, L.A. Perazolli, J.A. Varela, J. Eur. Ceram. Soc. 20 (2000) 1077-1084.
19 JCPDS, International Centre for Diffraction Data, 30-1468.
20 JCPDS, International Centre for Diffraction Data, 34-0394.
21 A. Fernandez, D. Haas, R.J.M. Konings, J. Somers, in: Proceedings of the NEA P&T Exchange Meeting 2000, Madrid, 2000.
22 H. Kinoshita, K. Kuramoto, U. Mazayoshi, T. Yanagi, S. Yamanaka, H. Mitamura, T. Banba, J. Am. Ceram. Soc. 83 (2000) 391-396.
23 K. Kuramoto, H. Mitamura, T. Banba, S. Muraoka, Prog. Nucl. Energy 32 (1998) 509-516.
24 A.A. Bukaemskiy, D. Barrier, D. Modolo, J. Eur. Ceram. Soc. 26 (2006) 1507-1515.
25 A. Aronne, A. Marotta, P. Pernice, M. Catauro, Therm. Acta 275 (1996) 75-82.
26 G.Y. Guo, Y.L. Chen, W.J. Ying, Mat. Chem. Phys., 84 (2004) 308-314.
27 M.C. Caracoche, P.C. Rivas, M.M. Cervera, R. Caruso, E. Benavidez, O. Sanctis, M.E. Escobar, J. Am. Ceram. Soc. 83 (2000) 377-384.